More Than Carbazole Derivative Activates Room Temperature Ultralong Organic Phosphorescence of Benzoindole Derivative

Authors: Chen Qian,[†,+] Zhimin Ma,[‡,+] Xiaohua Fu,[†] Xue Zhang,[†] Zewei Li,[‡] Huiwen Jin,[†] Mingxing Chen,[‡] Hong Jiang,[‡] Xinru Jia[‡] and Zhiyong Ma[†]*

Affiliations:

[†]Beijing Advanced Innovation Center for Soft Matter Science and Engineering, State Key Laboratory of Organic-Inorganic Composites, College of Chemical Engineering, Beijing University of Chemical Technology, Beijing 100029, China

[‡]Beijing National Laboratory for Molecular Sciences, Key Laboratory of Polymer Chemistry and Physics of the Ministry of Education, College of Chemistry and Molecular Engineering, Peking University, Beijing 100871, China

[+]These authors contributed equally.

*Correspondence to: mazhy@mail.buct.edu.cn.

Abstract: Herein, we report four carbazole/1H-benzo[f]indole (Cz/Bd) derivatives with increasing Bd substitution (Bd number=0~3), which give a general mechanism for Bd-based ultralong organic phosphorescence. To physically isolate Cz and Bd, we synthesized Cz and Bd in the lab, separately. According to experimental results, we draw several important points. **The first important point** is that Bd and its derivatives commonly possess two groups of intrinsic phosphorescence bands, of which short-lifetime band at ~450 nm is assigned to the molecular phosphorescence of their neutral molecules and of which typical ultralong phosphorescence bands at 560 nm, 610 nm and 660 nm are assigned to their radical cations. Amazingly, PMMA films (1wt.%) of CNCzBdBr and CN2BdBr both demonstrate photo-activated room-temperature ultralong organic phosphorescence while this doesn't happen to Bd and CN3Bd. **The second important point** is that activation of ultralong phosphorescence from Bd derivatives involves three factors: well dispersion with limited amount in matrix, generation of Bd derivatives' radical cations and stabilizing radical cations mediated by matrix. Cz derivative can function as a matrix to activate (room temperature) ultralong organic phosphorescence of Bd derivative but its activation function can be replaced by other methods such as photo-activation. **The third important point** is that the photo-activated ultralong organic phosphorescence is closely related to molecular structure of Bd derivative and stability of its radical cation. **The fourth important point** is that for double-carbazole system with trace isomer its room temperature ultralong organic phosphorescence originates at least from synergistic effect of monosubstituted product and disubstituted product of Bd. Furthermore, it is discovered that several other matrixes can also activate room-temperature ultralong organic phosphorescence of Bd derivatives, further verifying the second important point. To our best knowledge, this study is a big breakthrough in ultralong organic phosphorescence and will probably open a new era for its development.

Graphic Abstract: We successfully acquired four Cz/Bd derivatives (CN2CzBr, CNCzBdBr, CN2BdBr and CN3Bd) by using lab-synthesized Cz and lab-synthesized Bd. Bd and its derivatives feature double groups of intrinsic phosphorescence bands, of which the short-wavelength phosphorescence band is assigned to the molecular phosphorescence of Bd derivative and of which the ultralong phosphorescence at long wavelengths are ascribed to Bd derivative's radical cations. Fascinatingly, CNCzBdBr and CN2BdBr manifest photo-activated ultralong phosphorescence at room temperature in PMMA film but this doesn't happen to Bd and CN3Bd. Activation of room temperature ultralong phosphorescence from Bd derivatives involves three factors: well dispersion with limited amount in matrix, generation of Bd derivatives' radical cations and stabilizing radical cations mediated by matrix. Generally, the intrinsic ultralong phosphorescence of Bd derivatives can be activated by Cz derivatives. However, the activation function of Cz derivatives can be replaced by other methods such as photo-activation or other matrixes. Importantly, the photo-activated ultralong phosphorescence is closely related to molecular structure of Bd derivatives and stability of Bd derivatives' radical cations. Moreover, for some Cz systems synthesized from commercial Cz, their ultralong phosphorescence might originate from synergistic effect of two or even more Bd derivatives. This work might be a milestone in ultralong organic phosphorescence and open a new era for its development.

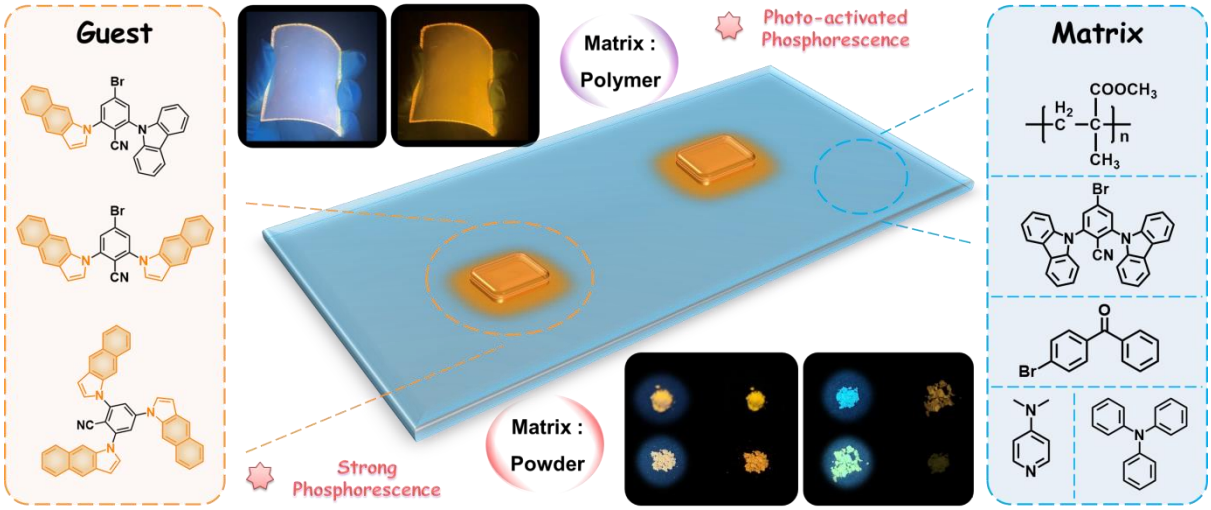

Main Text: Ultralong organic phosphorescence has been attracting considerable attention[1-3] in past years owing to its superiorities of low cost, low toxicity, flexible structral modification[4, 5] and easy color tunning,[6-11] and its wide applications in bio-imaging/sensing[12-15], encryption/anti-counterfeiting[16, 17] and organic light-emitting diode (OLED),[18, 19] *etc*. Carbazole (Cz) derivatives are promising light emitters or hole-transporting materials because of carbazole's coplannar configuration, which is conducive to electron comminication or charge carrier mobility.[20] Since that H-aggregation of carbazole derivatives stabilizes triplet excited states for ultralong organic phosphorescence was reported in 2015,[2] carbazole has become a star molecule in fabricating ultralong organic phosphorescence and hundreds of papers have been published.[21-27] However, recently Prof. Liu discovered that commercial carbazole contains trace carbazole isomer (1H-benzo[f]indole, Bd) and the isomer is convincingly involved in the origination of ultralong organic phosphorescence.[3, 28] They suggested that Cz and Bd moieties in close proximity could act as a microplanar heterojunction to generate photoinduced charge-separated states and further to produce intense ultralong organic phosphorescence. According to this research, the previously published results of ultralong organic phosphorescence from carbazole derivatives are actually integrated properties of pure carbazole derivatives and pure Bd's counterparts.[2, 14, 29-32] Unfortunately, the intrinsic photophysical property of pure Bd's counterpart, which is necessary for clearer elucidation of the mechanism for Cz&Bd-based ultralong organic phosphorescence, is still unclear because high pure Bd cannot be obtained by refining commercial Cz *via* HPLC and it is inevitable that the refined Bd contains trace carbazole. Thus, what's the

real truth of Cz&Bd-based ultralong organic phosphorescence?

To physically isolate Cz and Bd, we synthesized Cz and Bd in the lab, separately. Herein, we report four Cz/Bd derivatives (Figure 1a&1b), CN2CzBr with two carbazole units, CNCzBdBr with one carbazole and one benzoindole, CN2BdBr with two benzoindole groups and CN3Bd with three benzoindole moieties, which give a general mechanism for Bd-based ultralong organic phosphorescence. According to temperature-variable photoluminescence (PL) spectra, CN2CzBr in PMMA film (1 wt.%) shows molecular phosphorescence peaked at 439 nm, and the typical three phosphorescence bands over 550 nm (which were widely reported in previous carbazole system) were not detected; Interestingly, Bd, CNCzBdBr, CN2BdBr and CN3Bd in PMMA film (1wt.%) displayed two groups of phosphorescence bands, one of which was located at ~450 nm and the other of which were located at ~560 nm, ~610 nm, ~660 nm. **The first important point** is that Bd and its derivatives usually possess two groups of intrinsic phosphorescence bands, of which short-wavelength band is assigned to the molecular phosphorescence of Bd derivative and of which typical three phosphorescence bands are assigned to Bd derivative's radical cations. Amazingly, the PMMA films (1wt.%) of CNCzBdBr and CN2BdBr both demonstrated photo-activated room temperature ultralong organic phosphorescence at 560 nm, 610 nm and 660 nm while this didn't happen to the PMMA films of Bd and CN3Bd. Especially for CN2BdBr, without any Cz, the intense room-temperature ultralong organic phosphorescence still appeared after photo-activation. **The second important point** is that activation of room temperature ultralong phosphorescence from Bd derivatives involves three factors: well

dispersion with limited amount in matrix, generation of Bd derivatives' radical cations and stabilizing radical cations mediated by matrix. Cz derivative can function as a matrix to activate (room temperature) ultralong organic phosphorescence of Bd derivative but its activation function can be replaced by other methods. **The third important point** is that the photo-activated ultralong organic phosphorescence is closely related to molecular structure of Bd derivative and stability of Bd derivative's radical cations, which will open a new landscape for ultralong organic phosphorescence. Then, single component or multiple components of CNCzBdBr, CN2BdBr and CN3Bd was/were doped into CN2CzBr and the typical three phosphorescence bands appeared and enhanced remarkably. **The fourth important point** is that for double-carbazole system with trace isomer its room temperature ultralong organic phosphorescence originates at least from synergistic effect of monosubstituted product and disubstituted product of Bd. Furthermore, it is discovered that several other matrixes can also activate room-temperature ultralong organic phosphorescence of Bd derivatives, further verifying the second important point. To our best knowledge, this study is a big breakthrough in ultralong organic phosphorescence and will probably open a new era for its development.

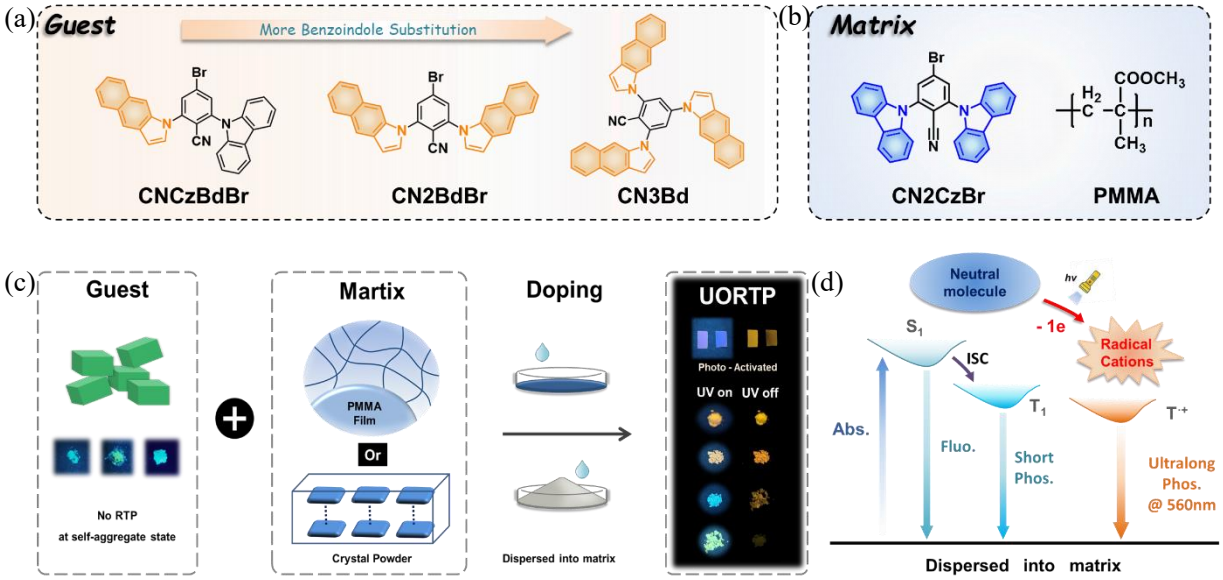

Figure 1. (a) Molecular structures of Bd derivatives (CNCzBdBr, CN2BdBr and CN3Bd) which function as guest; (b) molecular structures of CN2CzBr and PMMA which function as matrix; (c) (photo-activated) room temperature ultralong phosphorescence is lighted up when guest is doped into matrix; (d) proposed phosphorescence mechanism for Bd and Bd derivatives in matrix.

Results and Discussion

Synthesis and characterization. 1H-benzo[f]indole (Bd) was acquired as light yellow powder *via* seven-step reactions, starting from 3-amino-2-naphthoic acid (Scheme S1). Carbazole (Cz) was obtained as white powder through two-step reactions with aniline as the starting reagent. I have to stress that all the Bd and Cz used in this study are from lab synthesis without further declaration. CN2CzBr was afforded as white powder by typical substitution reaction between 4-bromo-2,6-difluorobenzonitrile and Cz. CN2BdBr and CN3Bd were both obtained as yellow powder *via* typical substitution reaction between 4-bromo-2,6-difluorobenzonitrile and Bd by controlling the reaction temperature.

Asymmetric CNCzBdBr was acquired as yellow powder by the way of CNCzBrF and then the substitution reaction between CNCzBrF and Bd. Also, CN2CzBr was synthesized with commercial Cz (named as CN2CzBr-com). ^{1}H NMR, ^{13}C NMR, HR-MS and crystallographic analyses were performed to verify the chemical structures of all the products. The detailed synthetic procedures and molecular characterization are available in the Supporting Information (Scheme S2, Figure S1-S20).

Photophysical properties in solution. Firstly, the photophysical properties of CN2CzBr, Bd, CNCzBdBr, CN2BdBr and CN3Bd were studied in THF solution (40 μM, Figure S21). Bd showed an absorbance band at 247 nm and another group of absorbance bands over 300 nm (at 330 nm, 345 nm and 361 nm), assigned to π→πn transition and n→πt transitions, respectively. CN2BdBr and CN3Bd possessed the similar absorbance bands with Bd. The π →πC transitions of CN2BdBr and CN3Bd were peaked at 242 nm and 243 nm, respectively. The n→πp transitions appeared at 310 nm, 356 nm and 387 nm for CN2BdBr and at 310 nm, 359 nm and 376 nm for CN3Bd. For CN2CzBr, its π→πo transition emerged at 229 nm and its n→πt transitions were located at 287 nm, 318 nm, 331 nm and 364 nm. For CNCzBdBr, its π→π transitions appeared at 236 nm with a shoulder band at 245 nm; and its n→πa transitions were located at 288 nm, 309 nm, 331 nm, 354 nm and 385 nm, exhibiting the integrated effect of Bd and Cz. In the photoluminescence spectra (Figure S21b), Bd's emission band was centered 391 nm, assigned to the locally excited (LE) fluorescence. The emission bands of CN2BdBr and CN3Bd were peaked at 460 nm and 482 nm, respectively, ascribed to intramolecular charge transfer (ICT) fluorescence; and their LE fluorescence bands, which should be similar with Bd, didn't appear. For CN2CzBr, its emission band was

peaked at 414 nm, assigned to the LE fluorescence, because this band is similar with the Cz's LE fluorescence. Moreover, CNCzBdBr displayed dual emissions at 411 nm and 496 nm, ascribed to LE fluorescence and ICT fluorescence, respectively.

Photophysical properties in solid state. Then, we investigated the solid-state luminescent properties of CN2CzBr, Bd, CNCzBdBr, CN2BdBr and CN3Bd (Figure S22). At room temperature, CN2CzBr showed two emission bands at 424 nm (5.36 μs) and 462 nm (3.04 ms) (Figure S23). In the temperature-variable PL spectra, intensity of the 424 nm emission band tended to decrease when temperature decreased from 317 K to 77 K (Figure S24), verifying its nature of thermally activated delayed fluorescence (TADF); a new emission band at 442 nm appeared and its intensity enhanced rapidly accompanied with the decrease of temperature, which is confirmed to be intrinsic molecular phosphorescence of CN2CzBr (later discussed in PMMA film section); and intensity of the 462 nm emission band strengthened sharply along with the cooling process, suggesting its assignment of crystalline phosphorescence. However, Bd, CNCzBdBr, CN2BdBr and CN3Bd all just showed weak fluorescence at 453 nm (4.09 ns, Figure S26), 480 nm (1.33 ns, Figure S25), 500 nm (6.39 ns, Figure S28) and 480 nm (1.85 ns, Figure S30); and no phosphorescence was detected at room temperature (Figure S22). At 77 K, CNCzBdBr and CN2BdBr exhibited ultralong yellow phosphorescence at 560 nm, 610 nm and 660 nm but the intensity was quite low (Figure S27&S29); even more, CN3Bd didn't show any ultralong phosphorescence at 77 K (Figure S31), indicating that it is not beneficial for ultralong phosphorescence when Bd or its derivatives self-aggregate.

Temperature-variable photophysical properties in PMMA film.

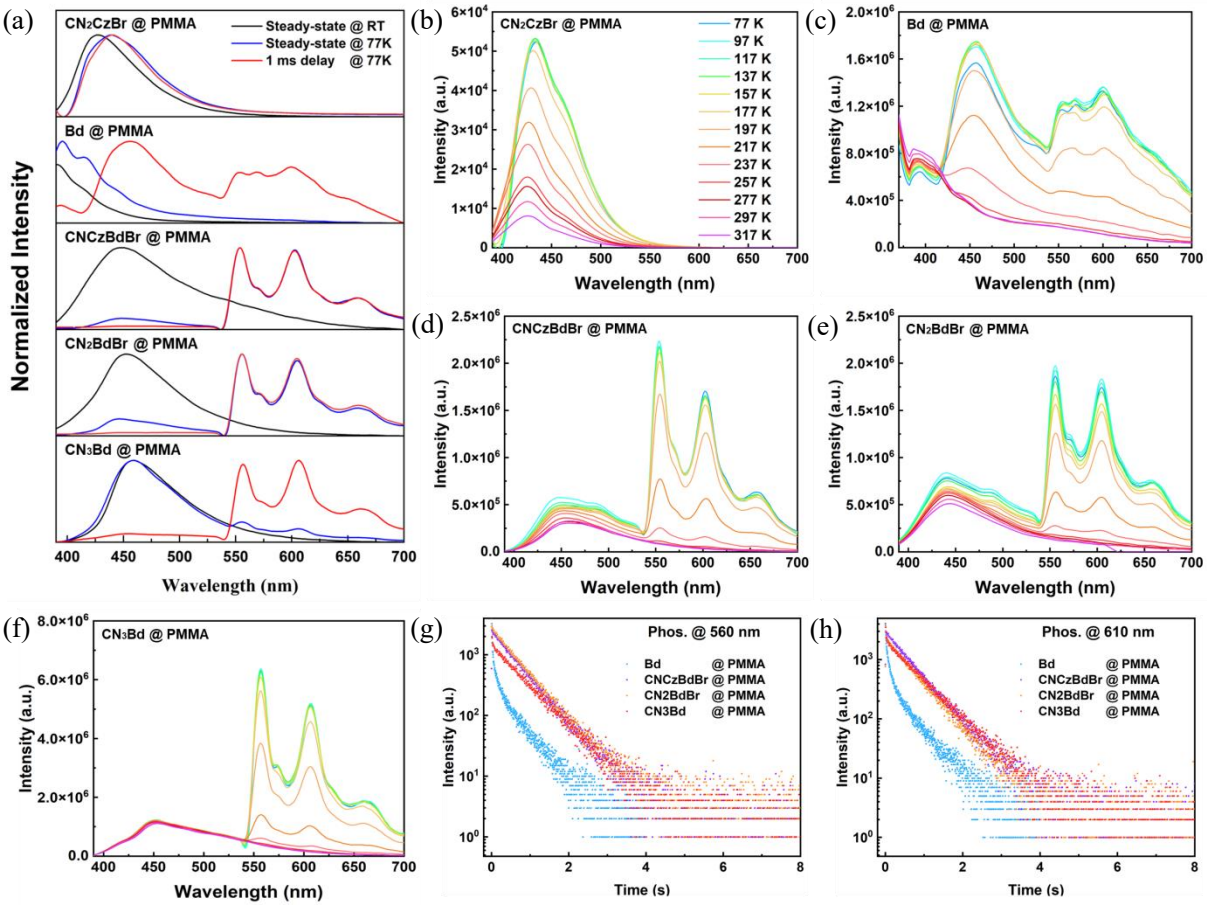

Figure 2. (a) Steady-state and delayed PL spectra at room temperature and at 77 K of CN2CzBr, Bd, CNCzBdBr, CN2BdBr and CN3Bd; temperature-variable PL spectra of (b) CN2CzBr (steady-state), (c) Bd (delayed), (d) CNCzBdBr (steady-state), (e) CN2BdBr (steady-state) and (f) CN3Bd (delayed); (g, h) decayed spectra at 560 nm and 610 nm of CN2CzBr, Bd, CNCzBdBr, CN2BdBr and CN3Bd at 77 K. All samples are PMMA films.

To study the intrinsic phosphorescence properties, CN2CzBr, Bd, CNCzBdBr, CN2BdBr and CN3Bd were doped into PMMA film with the weight ratio of 1%. PMMA film of CN2CzBr showed an emission band at 427 nm (Figure 2a) with the lifetime of 14.2 μs (Figure S32a) at room temperature, suggesting its nature of thermally activated delayed

fluorescence (TADF); and phosphorescence was not detected. At 77 K, its emission was centered at 439 nm (Figure 2a) with the lifetime of 70.9 ms (Figure S32b), assigned to molecular phosphorescence of CN2CzBr; and the typical three phosphorescence bands over 550 nm were not observed. In the temperature-variable PL spectra, the emission band red shifted from 427 nm to 439 nm and its intensity strengthened gradually along with the decrease of temperature (Figure 2b). Thus, the intrinsic molecular phosphorescence of CN2CzBr was located at 439 nm and the ultralong phosphorescence bands over 550 nm were not ascribed to CN2CzBr.

Surprisingly, Bd, CN2BdBr and CN3Bd all possess two groups of intrinsic phosphorescence bands at 77 K. At room temperature, the film of Bd showed a week fluorescence band at 391 nm (Figure 2a) with the lifetime of 8.25 ns (Figure S33) and no phosphorescence was detected. However, at 77 K, the fluorescence band at 391 nm still existed and two new groups of phosphorescence bands emerged (Figure 2b). The first group was located at 455 nm with the lifetime of 10.2 ms (Figure S33). The second group contained the typical three phosphorescence bands at 551 nm, 601 nm and 654 nm with the approximate lifetimes of 471.5 ms, 433.5 ms and 396.4 ms (Figure 2g&Figure S33). We put these three phosphorescence bands together as the group two because they usually emerge together and possess similar lifetimes. In the temperature-variable delayed PL spectra, these two groups of emission bands newly appeared and then enhanced gradually when temperature decreased (Figure 2c), verifying their characteristics of phosphorescence. As for CN2BdBr and CN3Bd, their PMMA films showed fluorescence bands (Figure 2a) at 455 nm with the lifetime of 3.88 ns (Figure S35) and 459 nm with the lifetime of 4.43 ns (Figure S36) at room temperature,

respectively; not any phosphorescence band was detected. At 77 K, CN2BdBr exhibited two groups of characteristic phosphorescence bands (Figure 2a). The short-wavelength group was centered at 446 nm with the lifetime of 17.15 ms (Figure S35); the long-wavelength group were the typical three phosphorescence bands at 554 nm (576.6 ms), 607 nm (570.1 ms) and 663 nm (572.1 ms) (Figure 2g&Figure S35). In the temperature-variable steady-state PL spectra, these two groups of emission bands newly appeared and then strengthened sharply with the decreasing temperature (Figure 2e), confirming their nature of phosphorescence. Also, CN3Bd displayed almost the same temperature-variable phosphorescence property as CN2BdBr (Figure 2f&S36). Though Bd, CN2BdBr and CN3Bd feature two similar groups of intrinsic phosphorescence bands, the relative intensity of each band was closely related to the molecular structure, especially for the typical three phosphorescence bands. According to Prof. Liu's work, it is rational that the typical three phosphorescence bands originated from Bd derivative's radical cation, which will be further confirmed by electron spin resonance (ESR) spectra; and we speculated that the short-wavelength phosphorescence was assigned to the intrinsic molecular phosphorescence of Bd derivative. These results tell us that the intrinsic phosphorescence of Bd derivatives might have nothing to do with Cz. Cooling can activate their intrinsic phosphorescence; Cz derivatives can also activate Bd derivatives' intrinsic phosphorescence but are not necessary for the activation.

CNCzBdBr is special because it is the first organic molecule constructed with both Cz and Bd. Then, the photophysical property of CNCzBdBr was also studied in PMMA film. At room temperature, its film showed a fluorescence band at 450 nm (1.39 ns, Figure 2a&Figure S34) and weak phosphorescence could be detected because of its unique photo-activation

(which will be discussed in detail hereinafter). At 77 K, two groups of phosphorescence bands dominated the PL spectra. The first group was located at 452 nm with the lifetime of 21.39 ms (Figure S34); the second group were also the typical three phosphorescence bands at 552 nm (575.6 ms), 604 nm (579.1 ms) and 661 nm (577.1 ms) (Figure 2g&Figure S34). The rapid enhancement in the temperature-variable steady-state PL spectra verified that these two groups of luminescence bands were indeed phosphorescence (Figure 2d). Interestingly, the intrinsic phosphorescence property of CNCzBdBr was almost the same as Bd, CN2BdBr and CN3Bd, implying that Bd dominated the phosphorescence-emitting process.

Photo-activated room-temperature ultralong organic phosphorescence. Marvellously, the PMMA films (1wt.%) of CNCzBdBr and CN2BdBr both manifested photo-activated room-temperature ultralong organic phosphorescence while this didn't happen to PMMA films of Bd and CN3Bd. The whole photo-activated processes of CNCzBdBr and CN2BdBr were present in Figure 3a. The as-prepared PMMA films were blue emitting and no afterglow was observed if portable UV light (365 nm, 16 W) was removed soon. When the portable UV light was kept on, the yellow ultralong phosphorescence of CNCzBdBr and CN2BdBr started to be lighted up at 9 s and 16 s; and their luminescence color both turned to yellowish. The phosphorescence-enhancing process of CNCzBdBr and CN2BdBr last 16 s and 20 s, respectively. At 77 s, when the UV light was switched off, both films displayed intense yellow afterglow. Then, we performed PL spectra to monitor the photo-activated process (Figure 3b&3c). The newly emerging phosphorescence bands after photo-activation were located at ~560 nm, ~610 nm and ~660 nm, ascribed to the intrinsic ultralong phosphorescence bands of their radical cations. When the scanning number increased, the

intensity of these phosphorescence bands enhanced remarkably, suggesting that the light source of fluorescence spectrophotometer could also activate these phosphorescence bands effectively. Furthermore, kinetic scanning of the photo-activated process was conducted. The photo-activation involved three stages (1, 2, 3 in Figure 3d). The stage 1 didn't witness the emergence of ultralong phosphorescence, which last 48 s for CNCzBdBr and 53 s for CN2BdBr. At stage 2, yellow ultralong phosphorescence newly appeared and its intensity enhanced gradually, which took 152 s for CNCzBdBr and 147 s for CN2BdBr. At stage 3 (from 200 s to 300 s), the intensity of ultralong phosphorescence kept unchanged. Compared with the initial state (with fluorescence only), the intensity of ultralong phosphorescence increased to 152.1% and 328.5% for CN2BdBr and CNCzBdBr (Figure 3e), respectively. The lifetimes of the photo-activated ultralong phosphorescence were tested to be 232.76 ms and 111.52 ms for CNCzBdBr and CN2BdBr (Figure 3f), respectively.

To illuminate the mechanism of photo-activated ultralong phosphorescence, electron spin resonance (ESR) spectra were performed. Before UV irradiation, no ESR signal was detected for both films of CNCzBdBr and CN2BdBr. After UV irradiation for 1 minute, obvious ESR signals appeared, which ranged from 3465 G to 3541 G for CNCzBdBr and from 3462 G to 3542 G for CN2BdBr (Figure 3g&3h), respectively. More interestingly, the ESR signals enhanced remarkably when UV irradiation last for 3 minutes (5 minutes for CN2BdBr). The *g* values of CNCzBdBr and CN2BdBr were calculated to be 2.0065 and 2.0064, which were very close to a free electron (2.0023), verifying that radical cations of CNCzBdBr and CN2BdBr were generated by photo-irradiation. Now, we could explain the process of photo-activation clearly. At stage 1, triplet oxygen in the film was cleared by photo. At stage

2, the radical cations of Bd derivatives began to generate and accumulate by photo irradiation. At stage 3, the quantity of radical cations became saturated because of their limited stability.

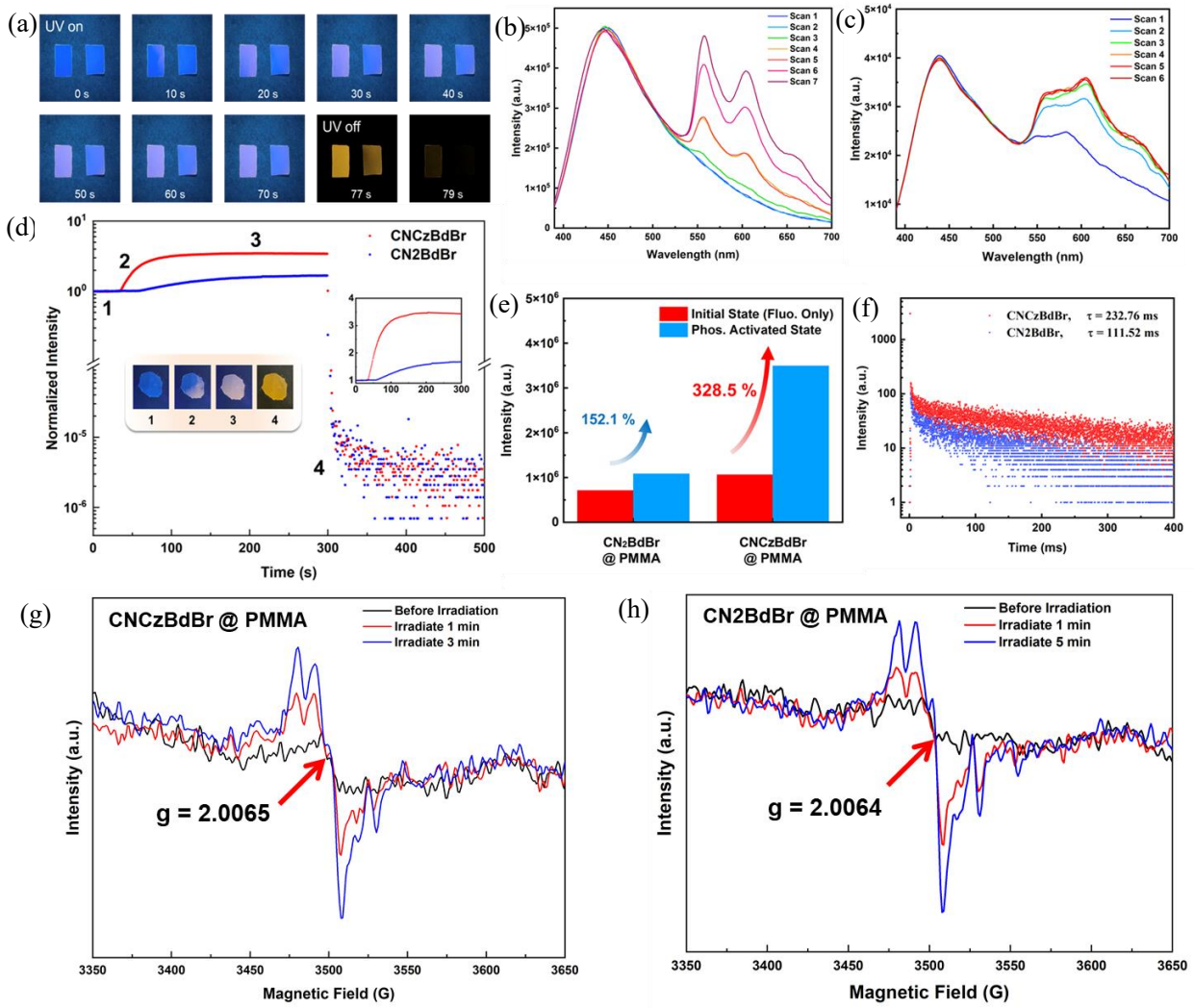

Figure 3. (a) Luminescent images of PMMA films of CNCzBdBr (left) and CN2BdBr (right) taken at different time point for the whole photo-activated process; photo-activated phosphorescence enhancement of CNCzBdBr (b) and CN2BdBr (c) in PMMA film monitored by steady-state PL spectra; (d) kinetic scannings of CNCzBdBr and CN2BdBr films; (e) intensity increase at 560 nm of CNCzBdBr and CN2BdBr films during kinetic scanning; (f) decay spectra at 560 nm of CNCzBdBr and CN2BdBr films after kinetic

scanning; ESR spectra of (g) CNCzBdBr and (h) CN2BdBr films before irradiation and after irradiation.

Moreover, the energy difference ($\Delta E = E_{M}^{\cdot+} - E_{M}$) between the neutral molecules (M) and corresponding radical cations ($M^{\cdot+}$) was calculated by using density function theory (DFT). Calculated ΔE of Bd, CNCzBdBr, CN2BdBr and CN3Bd were 573.16 kJ/mol, 448.02 kJ/mol, 430.84 kJ/mol and 419.86 kJ/mol (Figure 6c, Table S12), suggesting that the stability of $CNCzBdBr^{\cdot+}$, $CN2BdBr^{\cdot+}$ and $CN3Bd^{\cdot+}$ are relatively higher and it is easier for CNCzBdBr, CN2BdBr and CN3Bd to generate corresponding radical cations under photo irradiation. Besides high stability of radical cations, CN2BdBr and CN3Bd showed much higher intersystem crossing (ISC) efficiency than CN3Bd due to the heavy-atom effect. Therefore, CN2BdBr and CN3Bd exhibited remarkable photo-activated room temperature ultralong phosphorescence in PMMA film while Bd and CN3Bd didn't.

As commonly reported in previous carbazole systems with trace isomer,[33-36] the typical three ultralong phosphorescence bands at 560 nm, 610 nm and 660 nm usually emerged at room temperature, verifying that Cz derivatives can effectively activate intrinsic ultralong phosphorescence bands of Bd deritivatives' radical cations at room temperature. However, our results declare that intrinsic ultralong phosphorescence bands of Bd deritivatives' radical cations can also be activated by photo at room temperature and the activation function of Cz derivative can be totally replaced by other methods. Certainly, the photo-activated ultralong phosphorescence is closely related to molecular structures of Bd derivatives so more attention might be paied to discover new Bd derivatives to tune activation rate, PLQY and lifetime of

the ultralong phosphorescence.

Doping Bd derivatives into CN2CzBr. As discussed above, CN2CzBr, CNCzBdBr, CN2BdBr and CN3Bd all didn't show ultralong phosphorescence at room temperature. When doped into CN2CzBr, the intrinsic ultralong phosphorescence of all the three Bd derivatives were activated at room temperature (Figure S37~S39, Table S1~S3). After screening, the optimized doping ratio of CNCzBdBr@CN2CzBr, CN2BdBr@CN2CzBr and CN3Bd@CN2CzBr were 5%, 10% and 1% (Figure 4a&4b&4c) with maximal PLQY of 25.1%, 10.5% and 18.0% (Figure 4g), and corresponding lifetimes of 146.11 ms, 85.23 ms and 95.44 ms (of the 560 nm band, Figure 4e&4f), respectively. Comparing the three double-component systems, CN2CzBr could activate the intrinsic ultralong phosphorescence of CNCzBdBr more efficiently than CN2BdBr and CN3Bd. Furthermore, temperature-variable PL spectra were performed to gain deep insight into the CNCzBdBr@CN2CzBr system (5 wt.%). The typical three phosphorescence bands at 552 nm, 604 nm and 661 nm strengthened remarkably when temperature decreased from 317 K to 77 K (Figure 4d), verifying their nature of ultralong phosphorescence. During the cooling process, three emission bands at 427 nm, 451 nm and 468 nm split out, assigned to fluorescence/TADF of CN2CzBr, intrinsic phosphorescence of CNCzBdBr and crystalline phosphorescence of CN2CzBr, respectively. Thus, the luminescence property of CNCzBdBr@CN2CzBr was integration of the luminescence properties of CNCzBdBr and CN2CzBr.

Likewise, ESR spectra were carried out to evidence existence of radical cations in the

doped systems (Figure S43).[37, 38] For pure CN2CzBr powder, whether before UV irradiation or after UV irradiation, no ESR signal was detected, implying that no radicals were generated in pure CN2CzBr powder. For the doped systems CNCzBdBr@CN2CzBr, CN2BdBr@CN2CzBr and CN3Bd@CN2CzBr, ESR signal was observed even before UV irradiation, verifying that radical cations of Bd derivatives can exist stably in the matrix of CN2CzBr without photo-activation. Therefore, the ultralong phosphorescence of doped systems easily appeared without time-consuming photo-activation. After 5 min UV irradiation, the intensity of ESR signal increased a little, further suggesting that UV light can facilitate generation of radical cations.

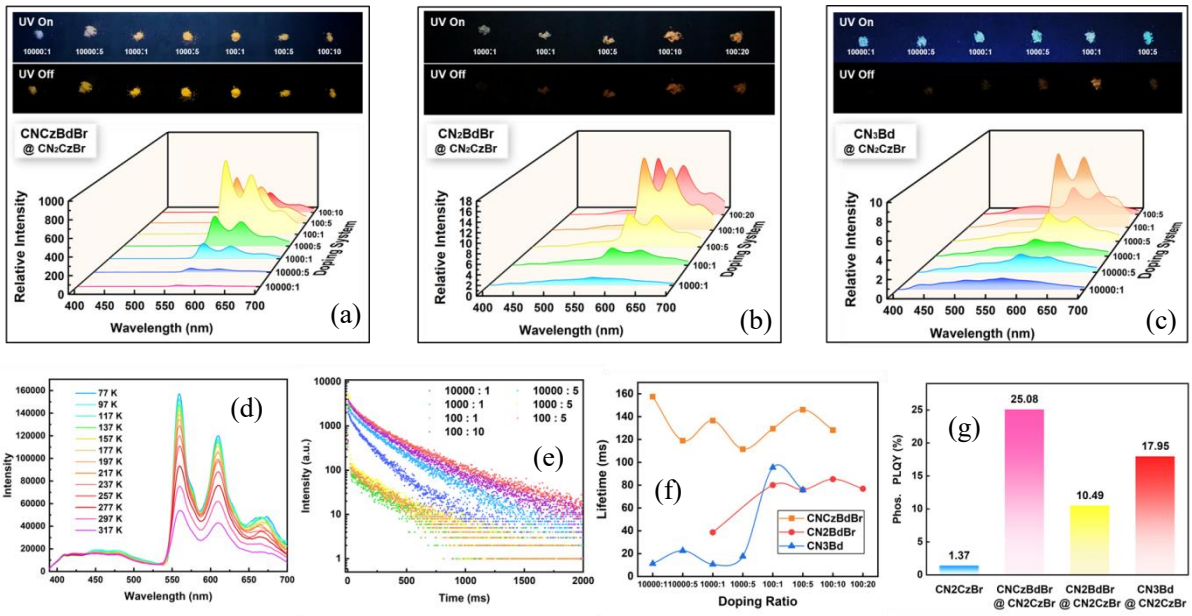

Figure 4. Luminescent and phosphorescent images, steady-state PL spectra at different dopant ratio for the doped system (a) CNCzBdBr@CN2CzBr, (b) CN2BdBr@CN2CzBr and (c) CN3Bd@CN2CzBr; (d) Temperature-variable steady-state spectra of CNCzBdBr@CN2CzBr (5wt.%); (e) decay spectra of CNCzBdBr@CN2CzBr with different

ratio; (f) lifetimes at 560 nm changed along with the dopant ratio for CNCzBdBr@CN2CzBr, CN2BdBr@CN2CzBr and CN3Bd@CN2CzBr; (g) Maximal PLQY of CNCzBdBr@CN2CzBr (5wt.%), CN2BdBr@CN2CzBr (10wt.%) and CN3Bd@CN2CzBr (1wt.%).

Our experimental results agreed well with Prof. Liu's work.[3, 28] Differently, the typical ultralong phosphorescence bands at 552 nm, 604 nm and 661 nm are the intrinsic phosphorescence of Bd derivatives' radical cations and CN2CzBr can activate their intrinsic ultralong phosphorescence probably by heterojunction. Formation of heterojunction requires close proximity between matrix and dopant, which is helpful in generating and stabilizing Bd derivatives' radical cations due to easy electron communication. With increasing Bd substitution, molecular geometry of Bd derivatives became more twisted. Higher structure similarity with CN2CzBr enabled CNCzBdBr and CN2CzBr to form effective heterojunction. Thus, the ultralong phosphorescence of CNCzBdBr can be activated more efficiently by CN2CzBr. Given higher ISC efficiency of CNCzBdBr, CNCzBdBr@CN2CzBr showed higher PLQY than CN2BdBr@CN2CzBr and CN3Bd@CN2CzBr. Moreover, for double-carbazole system (synthesized from commercial Cz), its room temperature ultralong organic phosphorescence originates at least from synergistic effect of monosubstituted product and disubstituted product of Bd (Figure S42).

Also, kinetic scannings of CNCzBdBr@CN2CzBr and CN2BdBr@CN2CzBr were conducted (Figure S40). However, after 300 s photo-irradiation, the intensity of ultralong phosphorescence (at ~560 nm) kept almost unchanged, implying that the intrinsic ultralong

phosphorescence of CNCzBdBr and CN2CzBr had been fully activated by CN2CzBr.

Other matrixes to activate room temperature ultralong phosphorescence. To replace the activation function of CN2CzBr, several other matrixes were studied. After screening, we found 4-bromobenzophenone (BBP), 4-(dimethylamino)pyridine (DMAP) and triphenylamine (TPA) could also activate the ultralong phosphorescence of CNCzBdBr at room temperature (Figure 5a). Pure BBP just showed weak blue fluorescence peaked at 450 nm and no afterglow was observed by naked eyes (Figure 5b&5c). When 1 wt.% of CNCzBdBr was doped into BBP, the doped system CNCzBdBr@BBP exhibited strong yellow ultralong phosphorescence at 560 nm, 610 nm and 660 nm with lifetimes of 101.18 ms, 92.55 ms and 88.12 ms (Figure 5d&5e&5f), implying that triplet excitons of CNCzBdBr's radical cations could also be stabilized by BBP. Pure DMAP displayed weak blue fluorescence centered at 450 nm and no ultralong phosphorescence band was detected (Figure 5b&5c). However, the doped system CNCzBdBr@DMAP witnessed the growth of yellow ultralong phosphorescence at 560 nm, 610 nm and 660 nm with lifetimes of 189.39 ms, 198.63 ms and 134.18 ms (Figure 5d&5e&5f). Interestingly, pure TPA showed weak blue fluorescence and green afterglow at 526 nm with lifetime of 87.99 ms (Figure 5b&5c&5d). Dramatically, there co-existed afterglow of TPA and ultralong phosphorescence bands of CNCzBdBr in the doped system CNCzBdBr@TPA, where the lifetime at 526 nm from TPA was 82.01 ms and the lifetimes at 560 nm, 610 nm and 660 nm from CNCzBdBr were 151.27 ms, 132.94 ms and 159.34 ms (Figure 5d&5e&5f). These results further confirm that Cz derivative function as a matrix to activate room temperature ultralong organic phosphorescence of Bd derivative and its activation function can be replaced by other

methods such as other matrixes.

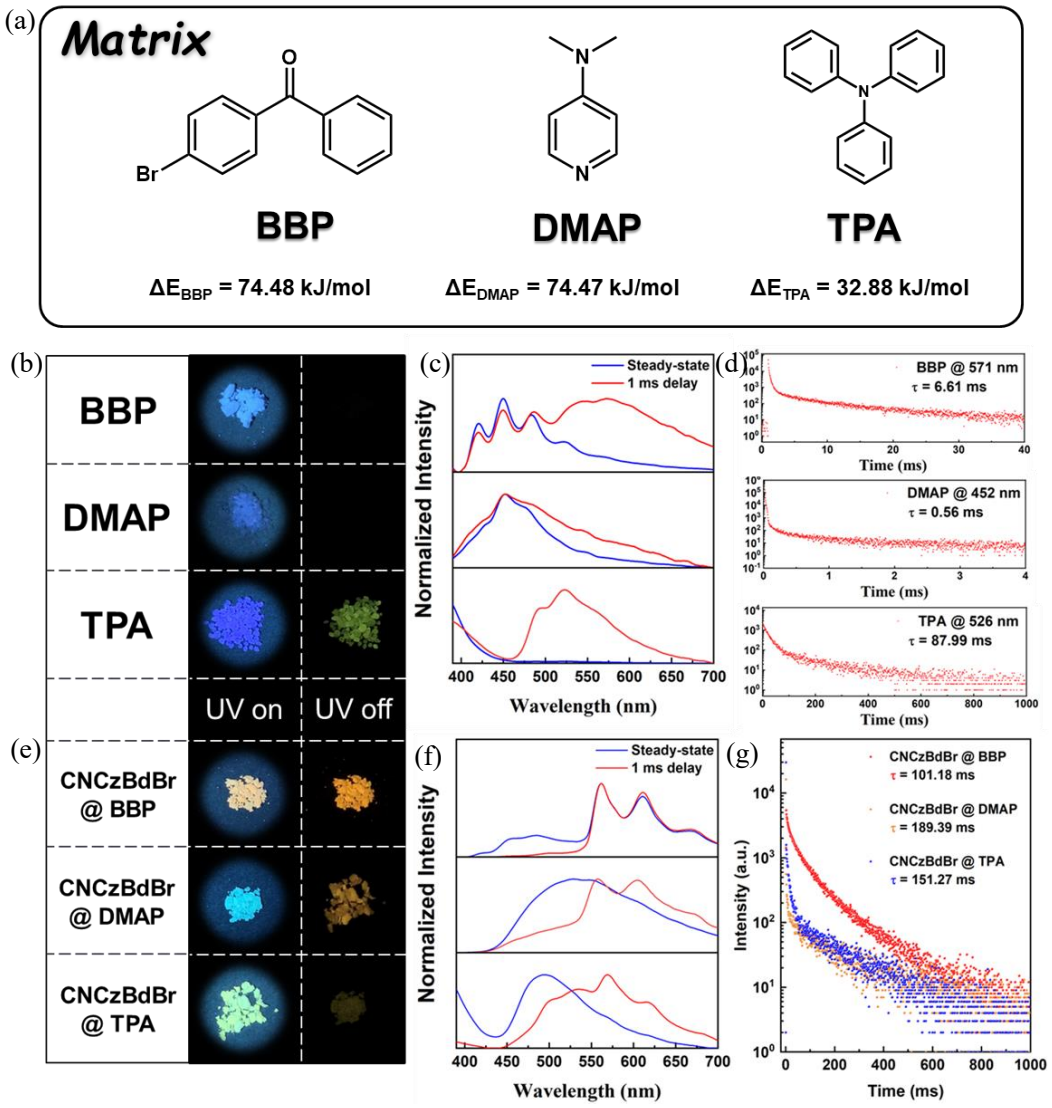

Figure 5. (a) Molecular structures of three matrixes BBP, DMAP and TPA; (b) luminescent and phosphorescent images, (c) steady-state and delayed PL spectra, (d) decay spectra of pure BBP, DMAP and TPA powder; (e) luminescent and phosphorescent images, (f) steady-state and delayed PL spectra, (g) decay spectra of doped system CNCzBdBr@BBP, CNCzBdBr@DMAP and CNCzBdBr@TPA.

Moreover, it was discovered that different matrix greatly affected intensity and lifetime of

the intrinsic ultralong phosphorescence bands of Bd derivatives. Probably, the electron-accepting ability of matrix is significant in generating and stabilizing Bd derivatives's radical cations. The energy difference ($\Delta E=E_{M}^{\cdot-}-E_{M}$) between the netural molecules (M) and corresponding radical ions ($M^{\cdot-}$) of matrix was calculated by using DFT. Calculated ΔE of CN2CzBr, BBP, DMAP and TPA were 119.82 kJ/mol, 74.48 kJ/mol, 74.47 kJ/mol and 32.88 kJ/mol (Table S13), suggesting that $CN2CzBr^{\cdot-}$, $BBP^{\cdot-}$, $DMAP^{\cdot-}$ and $TPA^{\cdot-}$ all exhibited good stability. However, other factors, for example, electron communication efficiency between matrix and guest, triplet oxygen in the matrix, may greatly influence final intensity of ultralong phosphorescence. Thus, all these matrixes can activate room temperature ultralong phosphorescence of CNCzBdBr but intensity of ultralong phosphoresnce is quite different. Therefore, exploring new matrixes to optimize the ultralong phosphorescence property of Bd derivatives and exploiting activation mechanism of different matrix will be an interesting topic.

TD-DFT calculations and proposed mechanism of ultralong phosphorescence. Furthermore, we employed time-dependent density function theory (TD-DFT) calculation to elucidate the intrinsic phosphorescence of Bd derivatives and the intrinsic ultralong phosphorescence of Bd derivatives' radical cations. On one hand, the S_1 of CN2CzBr in monomer state was calculated to be 2.998 eV (414 nm), in accordance with the experimental value (427 nm); the calculated T_1 and T_1* of CN2CzBr in monomer state and crystalline state were 2.898 eV (428 nm) and 2.895 eV (428 nm) (Figure 6a, Table S5, Figure S45&46), very close to our experimental results of 439 nm (molecular phosphorescence) and 462 nm (crystalline phosphorescence). No triplet energy level was found below 2.26 eV (550 nm),

suggesting that the ultralong phosphorescence bands over 550 nm are not from CN2CzBr. On the other hand, the S_n and T_n distributions of Bd derivatives were also calculated (Table S6-S11, Figure S47-S50). S_1 of CNCzBdBr, CN2BdBr and CN3Bd in monomer state were calculated to be 2.592 eV (478 nm), 2.587 eV (479 nm) and 2.646 eV (469 nm) (Figure 6a), agreeing well with the fluorescence bands of 450 nm for CNCzBdBr, 455 nm for CN2BdBr and 459 nm for CN3Bd. Considering spin orbital coupling (SOC) calculation and T_n distribution together, dominated T_n of CNCzBdBr, CN2BdBr and CN3Bd in monomer state were calculated to be 2.512 eV (T_2, 494 nm, $\langle S_1|Hso|T_2\rangle$=120.5 cm^{-1}, $\langle S_0|Hso|T_2\rangle$=366.4 cm^{-1}), 2.512 eV (T_3, 494 nm, $\langle S_1|Hso|T_3\rangle$=127.7 cm^{-1}, $\langle S_0|Hso|T_3\rangle$=373.8 cm^{-1}) and 2.587 eV (T_4, 479 nm, $\langle S_1|Hso|T_4\rangle$=0.36 cm^{-1}, $\langle S_0|Hso|T_4\rangle$=1.67 cm^{-1}) (Figure 6a), agreeing well with the experimental data (452 nm for CNCzBdBr, 446 nm for CN2BdBr and 452 nm for CN3Bd). Amazingly, there exists several excited states with strong oscillator strength in the range of 2.26 eV~1.65 eV (550 nm~750 nm) for radical cations of CNCzBdBr, CN2BdBr and CN3Bd (Figure 6b, Figure S51-S54), verifying that the ultralong phosphorescence bands over 550 nm originate from Bd derivatives' radical cations. SOC calculation also showed that the intersystem crossing (ISC) efficiency of CNCzBdBr and CN2BdBr were much higher than CN3Bd owing to heavy-atom effect so photo-activated room-temperature ultralong phosphorescence was not observed in PMMA film of CN3Bd (Table S10). TD-DFT results further confirmed that the short-wavelength phosphorescence band (at ~450 nm) was assigned to molecular phosphorescence of Bd derivative and the long-wavelength ultralong phosphorescence bands (over 550 nm) were ascribed to Bd derivative's radical cations.

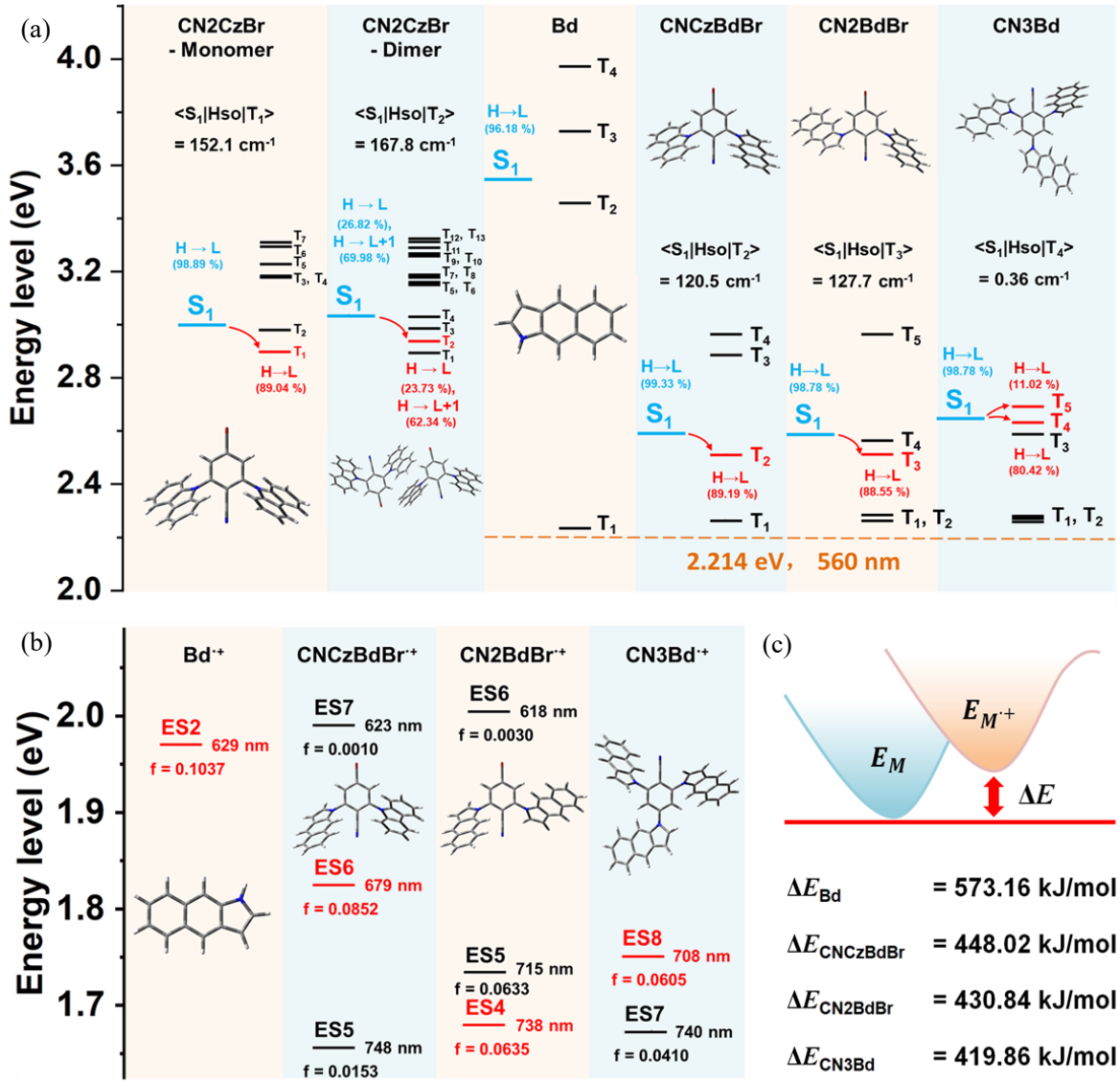

Figure 6. (a) The energy level diagrams for monomer and dimer of CN2CzBr, Bd, CNCzBdBr, CN2BdBr and CN3Bd; (b) the energy level diagrams for $Bd^{\cdot+}$, $CNCzBdBr^{\cdot+}$, $CN2BdBr^{\cdot+}$ and $CN3Bd^{\cdot+}$; (c) the energy gap between neutral molecule and corresponding racial cation for Bd, CNCzBdBr, CN2BdBr and CN3Bd.

On the basis of the theoretical and experimental data, the phosphorescence mechanism of Bd derivatives were proposed as shown in Figure 1c&1d. **Three necessary conditions should be satisfied to activate room temperature ultralong phosphorescence of Bd derivatives**. Firstly, Bd derivatives should be dispersed into matrixes to prevent their

self-aggregation which will quench phosphorescence. Secondly, the generation of Bd derivatives' radical cations is indispensable and photo-irradiation facilitates their generation. Thirdly, the Bd derivatives' radical cations should be stabilized by matrixes and matrixes greatly affect lifetime and PLQY of the ultralong phosphorescence.

Application demonstration of photo-activated ultralong phosphorescence.

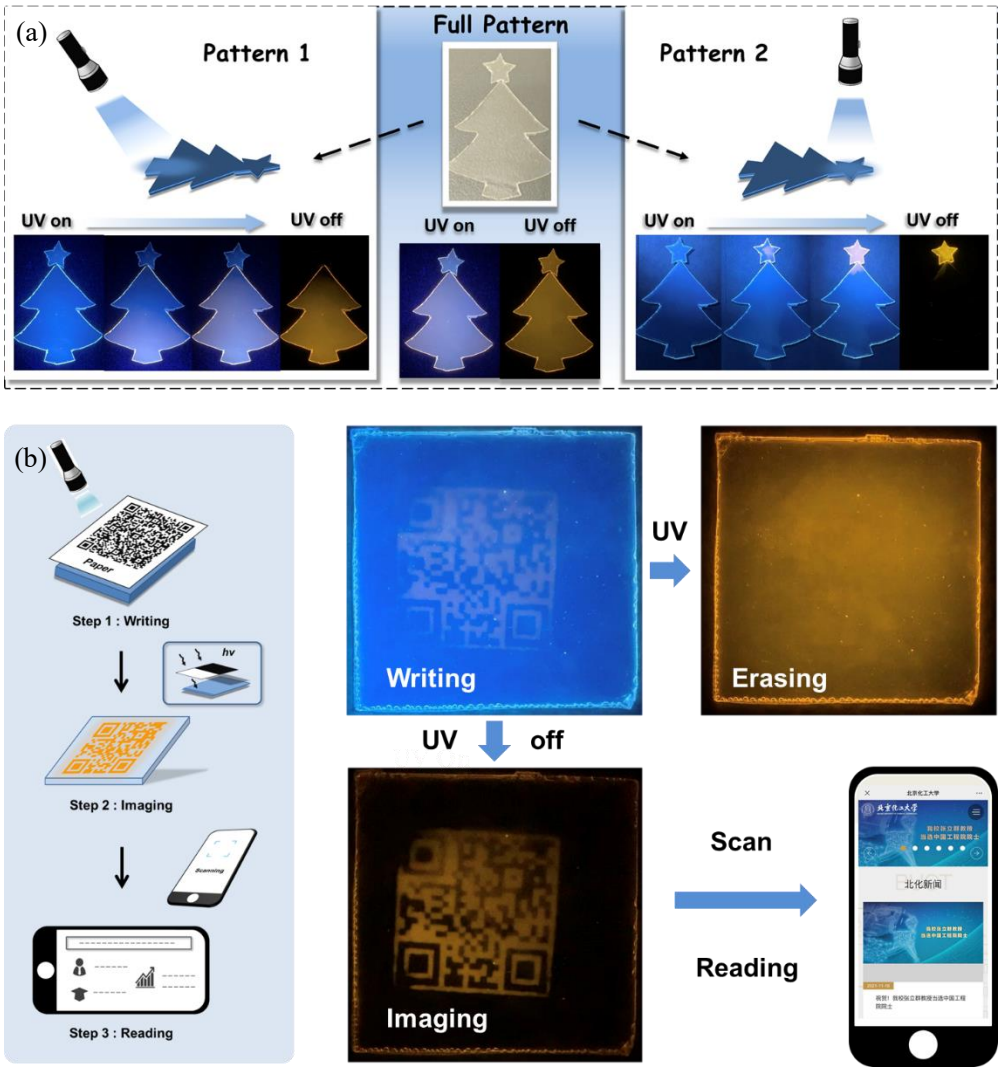

Figure 7. Applications of photo-activated ultralong phosphorescence (PMMA films doped with CNCzBdBr).

Applications of photo-activated ultralong phosphorescence in doped PMMA film were

demonstrated. The doped PMMA films can be prepared on a large scale facilely. Firstly, the doped PMMA film can be tailored into various shapes. As shown in Figure 7a, a Christmas tree was cut out. When different part of the tree was irradiated by 365 nm UV light, the selected part would be lighted up with yellow afterglow. Amazingly, the doped PMMA films exhibited high sensitivity to irradiation intensity. For example, a QR code was printed on a A4 white paper in black and white; then a doped PMMA film was covered by the A4 paper; when UV light irradiated the pattern above the A4 paper, the pattern would be printed on the PMMA film and further give out yellow afterglow (Figure 7b). The photo-printed yellow pattern displayed high resolution and the QR code could be successfully scanned by cellphones. Also, the QR code could be erased by further irradiation and the PMMA film could recover to initial state in less than 5 minutes at ambient condition.

Conclusion

In summary, we successfully acquired four Cz/Bd derivatives (CN2CzBr, CNCzBdBr, CN2BdBr and CN3Bd) by using lab-synthesized Cz and lab-synthesized Bd. Bd and its derivatives feature double groups of intrinsic phosphorescence bands, of which the short-wavelength phosphorescence band is assigned to the molecular phosphorescence of Bd derivative and of which the ultralong phosphorescence at long wavelengths are ascribed to Bd derivative's radical cations. Fascinatingly, CNCzBdBr and CN2BdBr manifest photo-activated intrinsic ultralong phosphorescence at room temperature in PMMA film but this doesn't happen to Bd and CN3Bd. Activation of room temperature ultralong phosphorescence from Bd derivatives involves three factors: well dispersion with limited

amount in matrix, generation of Bd derivatives' radical cations and stabilizing radical cations mediated by matrix. Generally, the intrinsic ultralong phosphorescence of Bd derivatives can be activated by Cz derivatives. However, the activation function of Cz derivatives can be replaced by other methods such as photo-activation or other matrixes. Importantly, the photo-activated ultralong phosphorescence is closely related to molecular structure of Bd derivatives and stability of Bd derivatives' radical cations so screening novel structures to optimize ultralong phosphorescence property is of great significance. Moreover, for some Cz systems synthesized from commercial Cz, their ultralong phosphorescence might originate from synergistic effect of two or even more Bd derivatives. This work might be a milestone in ultralong organic phosphorescence and open a new era for its development.

Methods

Synthesis of Bd. The synthetic detail of ISO 1-5 is shown in Supporting Information. ISO-6 (0.8361 g, 5 mmol) was dissolved in pyridine (10 mL) in a Schlenk bottle. The mixed solution was refluxed at 90 ℃ for 1 h under N_2 atmosphere. The crude product was purified by column chromatography using dichloromethane and petroleum ether (v/v, 1:2) as the eluent to obtain pure product as light yellow powder. Yield: 99%.

^{1}H NMR (400 MHz, $CDCl_3$) δ (ppm) : 8.21 (s, 1H), 7.98 (dd, J = 32.0, 8.0 Hz, 3H), 7.78 (s, 1H), 7.49 – 7.35 (m, 3H), 6.73 (s, 1H).

^{13}C NMR (400 MHz, $CDCl_3$) δ (ppm) : 136.57, 130.32, 129.62, 128.78, 128.28, 128.21, 127.31, 123.75, 122.61, 118.09, 106.23, 102.02.

HR-ESI-MS Calcd. For $C_{12}H_{10}N$ $[M+H]^+$: 168.0813. Found: 168.0815.

CN2CzBr: A mixture of Carbazole (1.8393 g, 11 mmol), 4-bromo-2,6-difluorobenzonltrlle

(1.0900 g, 5 mmol) and t-BuOK (1.3465 g, 12 mmol) were dissolved in DMF (10 mL) in a Schlenk bottle and was stirred under N_2 atmosphere for 24 h at 110 °C. After the reaction was over, the resultant mixture was cooled down to room temperature and the solvent was removed under reduced pressure. The crude product was purified by column chromatography using dichloromethane and petroleum ether (v/v, 1:5) as the eluent to obtain pure product as white powder. Yield: 68%.

^{1}H NMR (400 MHz, $CDCl_3$) δ (ppm) : 8.18 – 8.13 (m, 4H), 7.93 (s, 2H), 7.52 (td, J = 7.5, 1.1 Hz, 4H), 7.38 (dd, J = 8.1, 6.1 Hz, 8H).

^{13}C NMR (101 MHz, $CDCl_3$) δ (ppm) : 143.62, 140.34, 131.92, 129.07, 126.60, 124.32, 121.55, 120.84, 112.77, 111.81, 109.69.

HR-ESI-MS Calcd. For $C_{31}H_{19}N_3Br$ $[M+H]^+$: 512.0762. Found: 512.0763.

CN2BdBr: A mixture of 4-bromo-2,6-difluorobenzonltrlle (0.2398 g, 1.1 mmol), **1H-benzo[f]indole** (0.3679 g, 2.2 mmol) and t-BuOK (0.3366 g, 3 mmol) were dissolved in DMF (10 mL) in a Schlenk bottle and was stirred under N_2 atmosphere for 24 h at room temperature. After the reaction was over, the solvent was removed under reduced pressure. The crude product was purified by column chromatography using dichloromethane and petroleum ether (v/v, 1:5) as the eluent to obtain pure product as yellow powder. Yield: 36%.

^{1}H NMR (400 MHz, $CDCl_3$) δ (ppm): 8.23 (s, 2H), 8.12 (s, 1H), 8.00 (dd, J = 18.0, 6.5 Hz, 7H), 7.70 (d, J = 3.6 Hz, 2H), 7.53 – 7.42 (m, 4H), 6.99 (dd, J = 11.7, 6.0 Hz, 2H).

^{13}C NMR (101 MHz, $CDCl_3$) δ (ppm): 145.21, 136.36, 131.37, 130.77, 130.41, 129.75, 128.88, 128.26, 127.91, 127.64, 124.83, 123.88, 119.56, 106.17, 106.02.

HR-ESI-MS Calcd. For $C_{31}H_{19}N_3Br$ $[M+H]^+$: 512.0762. Found: 512.0763.

CN3Bd: A mixture of **1H-benzo[f]indole** (0.0501 g, 0.3 mmol), 4-bromo-2,6-difluorobenzonltrlle (0.0218 g, 0.1 mmol) and t-BuOK (0.0449 g, 0.4 mmol) were dissolved in DMF (2 mL) in a Schlenk tube and was stirred under N_2 atmosphere for 24 h at 110 °C. After the reaction was over, the resultant mixture was cooled down to room temperature and the solvent was removed under reduced pressure. The crude product was purified by column chromatography using dichloromethane and petroleum ether (v/v, 1:3) as the eluent to obtain pure product as yellow powder. Yield: 52%.

^{1}H NMR (400 MHz, $CDCl_3$) δ (ppm): 8.34 (s, 1H), 8.27 (s, 2H), 8.21 (s, 1H), 8.17 (s, 2H), 8.09 (s, 2H), 8.07 – 7.92 (m, 6H), 7.83 (d, J = 3.6 Hz, 2H), 7.66 (d, J = 3.6 Hz, 1H), 7.56 – 7.41 (m, 6H), 7.03 (d, J = 3.6 Hz, 2H), 6.98 (d, J = 3.5 Hz, 1H).

^{13}C NMR (101 MHz, $CDCl_3$) δ (ppm): 145.71, 136.69, 135.23, 131.90, 130.75, 130.50, 129.63, 128.18, 128.03, 127.76, 127.53, 124.91, 124.71, 124.05, 123.72, 119.57, 119.28, 118.68, 106.81, 106.66, 106.21, 105.24.

HR-ESI-MS Calcd. For $C_{43}H_{27}N_4$ $[M+H]^+$: 599.2236. Found: 599.2247.

Synthesis of CNCzBdBr. A mixture of **CNCzBrF** (0.2950 g, 0.8 mmol), **1H-benzo[f]indole** (0.1350 g, 0.8 mmol) and K_2CO_3 (0.1670 g, 1.2 mmol) were dissolved in DMF (10 mL) in a Schlenk bottle and was stirred under N_2 atmosphere for 24 h at room temperature. After the

reaction was over, the solvent was removed under reduced pressure. The crude product was purified by column chromatography using dichloromethane and petroleum ether (v/v, 1:5) as the eluent to obtain pure product as yellow powder. Yield: 85%.

^{1}H NMR (400 MHz, $CDCl_3$) δ (ppm) : 8.23 (s, 1H), 8.19 (d, J = 8.1 Hz, 2H), 8.11 (d, J = 1.6 Hz, 1H), 8.00 (dd, J = 13.2, 8.8 Hz, 3H), 7.83 (d, J = 1.6 Hz, 1H), 7.73 (d, J = 3.6 Hz, 1H), 7.56 – 7.44 (m, 4H), 7.43 – 7.36 (m, 4H), 6.97 (d, J = 3.6 Hz, 1H).

^{13}C NMR (101 MHz, $CDCl_3$) δ (ppm) : 145.07, 143.78, 140.31, 136.27, 131.36, 130.78, 130.45, 130.29, 129.79, 129.06, 128.27, 127.66, 126.54, 124.88, 124.29, 123.93, 121.51, 120.82, 119.62, 113.51, 109.81, 108.20, 106.16.

HR-ESI-MS Calcd. For $C_{31}H_{19}N_3Br$ $[M+H]^+$: 512.0762. Found: 512.0759.

Data availability. All data that support the findings of this study are available in the online version of this paper in the accompanying Supplementary Information (including experimental methods/procedures, synthetic routes, molecular characterization of Bd/CN2CzBr/CNCzBdBr/CN2BdBr/CN3Bd, photophysical properties in solution and in solid state, PL spectra of doped PMMA films, PL spectra of doped CN2CzBr, single crystal data, TD-DFT results).

References

1. Ye, W., et al. Confining isolated chromophores for highly efficient blue phosphorescence. *Nat. Mater.* **20,** 1539-1544(2021).

2. An, Z., et al. Stabilizing triplet excited states for ultralong organic phosphorescence. *Nat. Mater.* **14,** 685-690(2015).

3. Chen, C., et al. Carbazole isomers induce ultralong organic phosphorescence. *Nat. Mater.* **20,** 175-180(2021).

4. Liao, Q., et al. 9,9-Dimethylxanthene Derivatives with Room-Temperature Phosphorescence. *Angew. Chem. Int. Ed.* **59,** 1-6(2020).

5. Wen, Y., et al. Achieving Highly Efficient Pure Organic Single-Molecule White-Light Emitter: The Coenhanced Fluorescence and Phosphorescence Dual Emission by Tailoring Alkoxy Substituents. *Adv. Opt. Mater.* **8,** 1901995(2020).

6. Gu, L., et al. Color-tunable ultralong organic room temperature phosphorescence from a multicomponent copolymer. *Nat. Commun.* **11,** 944(2020).

7. Zheng, H., Wang Y., Cao P., Wu P. Color-tunable ultralong room temperature phosphorescence from EDTA. *Chem. Commun. (Camb.)* **57,** 3575-3578(2021).

8. Li, H., et al. Fluorine-induced aggregate-interlocking for color-tunable organic afterglow with a simultaneously improved efficiency and lifetime. *Chem. Sci.* **12,** 3580-3586(2021).

9. Wang, J., et al. Time dependent afterglow color in a single component organic molecualr crystal. *Angew Chem Int Ed.* **59,** 10032-10036(2020).

10. Bi, X., et al. Multi-Stimuli Responsive and Multicolor Adjustable Pure Organic Room Temperature Fluorescence-Phosphorescent Dual-Emission Materials. *Adv. Funct. Mater.* **31,** 2101312(2021).

11. Gu, L., et al. Colour-tunable ultra-long organic phosphorescence of a single-component molecular crystal. *Nat. Photonics* **13,** 406-411(2019).

12. Jin, J., et al. Thermally activated triplet exciton release for highly efficient tri-mode organic afterglow. *Nat. Commun.* **11,** 842(2020).

13. Gao, H., et al. Boosting Room Temperature Phosphorescence Performance by Alkyl Modification for Intravital Orthotopic Lung Tumor Imaging. *Small* **17,** e2005449(2021).

14. Zhen, X., et al. Ultralong Phosphorescence of Water-Soluble Organic Nanoparticles for In Vivo Afterglow Imaging. *Adv. Mater.* **29,** 1606665(2017).

15. Xu, L., et al. Ultralong Organic Phosphorescent Nanocrystals with Long-Lived Triplet Excited States for Afterglow Imaging and Photodynamic Therapy. *ACS Appl. Mater. Interfaces* **12,** 18385-18394(2020).

16. Gu, L., et al. Circularly Polarized Organic Room Temperature Phosphorescence from Amorphous Copolymers. *J. Am. Chem. Soc.* **143,** 13675-13685(2021).

17. Yang, Y. D., et al. Time-dependent solid-state molecular motion and colour tuning of host-guest systems by organic solvents. *Nat. Commun.* **11,** 77(2020).

18. Hu, J., et al. Single White-Emitting Polymers with High Efficiency, Low Roll-Off, and Enhanced Device Stability by Using Through-Space Charge Transfer Polymer with Blue Delayed Fluorescence as Host for Yellow Phosphor. *Adv. Opt. Mater.* **8,** 1902100(2020).

19. Wang, J., et al. A facile strategy for realizing room temperature phosphorescence and single molecule white light emission. *Nat. Commun.* **9,** 2963(2018).

20. Yang, Z., et al. Boosting the Quantum Efficiency of Ultralong Organic Phosphorescence up to 52 % via Intramolecular Halogen Bonding. *Angew. Chem. Int. Ed.* **59,** 17451-17455(2020).

21. He, Z., et al. Achieving Persistent, Efficient, and Robust Room-Temperature Phosphorescence from Pure Organics for Versatile Applications. *Adv. Mater.* **31,** e1807222(2019).

22. Gao, W., et al. Effect of Carbazolyl Groups on Photophysical Properties of Cyanuric

Chloride. *ACS Appl. Mater. Interfaces* **11,** 47162-47169(2019).

23. Gan, N., et al. Manipulating the Stacking of Triplet Chromophores in the Crystal Form for Ultralong Organic Phosphorescence. *Angew. Chem. Int. Ed. Engl.* **58,** 14140-14145(2019).

24. Xiong, Y., et al. Designing Efficient and Ultralong Pure Organic Room-Temperature Phosphorescent Materials by Structural Isomerism. *Angew. Chem. Int. Ed. Engl.* **57,** 7997-8001(2018).

25. Liu, Y., et al. Robust White-Light Emitting and Multi-Responsive Luminescence of a Dual-Mode Phosphorescence Molecule. *Adv. Opt. Mater.* **9,** 2001685(2021).

26. Huang, L., et al. Crystal-State Photochromism and Dual-Mode Mechanochromism of an Organic Molecule with Fluorescence, Room-Temperature Phosphorescence, and Delayed Fluorescence. *Angew. Chem. Int. Ed.* **58,** 16445-16450(2019).

27. Kenry, Chen C., Liu B. Enhancing the performance of pure organic room-temperature phosphorescent luminophores. *Nat. Commun.* **10,** 2111(2019).

28. Chen, C., et al. Revisiting Carbazole: Origin, Impurity, and Properties. *ACS Mater. Lett.* **3,** 1081-1087(2021).

29. Xie, Y., et al. How the Molecular Packing Affects the Room Temperature Phosphorescence in Pure Organic Compounds: Ingenious Molecular Design, Detailed Crystal Analysis, and Rational Theoretical Calculations. *Adv. Mater.* **29,** 1606829(2017).

30. Cai, S., et al. Enhancing Ultralong Organic Phosphorescence by Effective π-Type Halogen Bonding. *Adv. Funct. Mater.* **28,** 1705045(2018).

31. Gu, L., et al. Dynamic Ultralong Organic Phosphorescence by Photoactivation. *Angew. Chem. Int. Ed.* **57,** 8425-8431(2018).

32. Wang, X., et al. Organic phosphors with bright triplet excitons for efficient X-ray-excited luminescence. *Nat. Photonics* **15,** 187-192(2021).

33. Yuan, J., et al. Invoking ultralong room temperature phosphorescence of purely organic compounds through H-aggregation engineering. *Mater. Horiz.* **6,** 1259-1264(2019).

34. Feng, H. T., et al. Tuning molecular emission of organic emitters from fluorescence to phosphorescence through push-pull electronic effects. *Nat. Commun.* **11,** 2617(2020).

35. Shi, H., et al. Highly Efficient Ultralong Organic Phosphorescence through Intramolecular-Space Heavy-Atom Effect. *J. Phys. Chem. Lett.* **10,** 595-600(2019).

36. Liang, X., et al. Organic Room-Temperature Phosphorescence with Strong Circularly Polarized Luminescence Based on Paracyclophanes. *Angew. Chem. Int. Ed. Engl.* **58,** 17220-17225(2019).

37. Mu, Y., et al. Sensitive and Repeatable Photoinduced Luminescent Radicals from A Simple Organic Crystal. *Angew. Chem. Int. Ed. Engl.* **60,** 6367-6371(2021).

38. Yang, Y., et al. Tunable Photoresponsive Behaviors Based on Triphenylamine Derivatives: The Pivotal Role of pi-Conjugated Structure and Corresponding Application. *Adv. Mater.* **33,** e2104002(2021).

39. Li, J., et al. Transient and Persistent Room-Temperature Mechanoluminescence from a White-Light-Emitting AIEgen with Tricolor Emission Switching Triggered by Light. *Angew. Chem. Int. Ed.* **57,** 6449-6453(2018).

Acknowledgements

This work is financially supported by the National Natural Science Foundation of China (22175015, 21704002), the Beijing Natural Science Foundation (2182054), the Big Science Project from BUCT (XK180301), and the Fundamental Research Funds for the Central Universities to Z. Y. Ma.

Author contributions

C.Q., Z.M.M., X.H.F., X.Z., Z.W.L. and H.W.J. performed the experiments and prepared the Supplementary Information. Z.Y.M. conceived and directed the project. Z.Y.M. and Z.M.M. wrote the manuscript. X.R.J. and H.J. helped modified the manuscript.

Competing financial interests: The authors declare no competing financial interests.